# Charge transfer excitons and image potential states on organic semiconductor surfaces

Qingxin Yang, Matthias Muntwiler, and X.-Y. Zhu*
*Department of Chemistry, University of Minnesota, Minneapolis, Minnesota 55455, USA*
(Received 16 May 2009; revised manuscript received 12 August 2009; published 24 September 2009)

We report two types of excited electronic states on organic semiconductor surfaces: image potential states (IPS) and charge transfer excitons (CTE). In the former, an excited electron is localized in the surface-normal direction by the image potential and delocalized in the surface plane. In the latter, the electron is localized in all directions by both the image potential and the Coulomb potential from a photogenerated hole on an organic molecule. We use crystalline pentacene and tetracene surfaces as model systems, and time- and angle-resolved two-photon photoemission spectroscopy to probe the energetics and dynamics of both the IPS and the CTE states. On either pentacene or tetracene surfaces, we observe delocalized image bands and a series of CT excitons with binding energies $<0.5$ eV below the image-band minimum. The binding energies of these CT excitons agree well with solutions to the atomic-H-like Schrödinger equation based on the image potential and the electron-hole Coulomb potential. We hypothesize that the formation of CT excitons should be general to the surfaces of organic semiconductors where the relatively narrow valance-band width facilitates the localization of the hole and the low dielectric constant ensures strong electron-hole attraction.

DOI: 10.1103/PhysRevB.80.115214 PACS number(s): 71.35.−y, 72.40.+w, 73.20.−r

## I. INTRODUCTION

It is well established that the surface of a polarizable material supports a series of image potential states (IPS) or resonances.[1] The origin of an IPS can be easily understood when one considers an excess electron above a surface. Polarization by the excess electron creates a positive charge distribution in the near-surface region. Solution to the Poisson equation tells us that the interaction between the excess electron and the polarization cloud is equivalent to the Coulomb attraction between the electron above an image plane (often approximated by the physical surface) and a fictitious image charge at equal distance below the image plane. Depending on the band structure of the material, the image potential gives rise to a series of either image states or image resonances characterized by atomic-H-like principal quantum numbers. Image potential states have been extensively investigated in the past, particularly on single-crystal metal surfaces. In experimental studies, an electron in an IPS is most often populated by optical excitation from an occupied band of the metal substrate. Due to the high density of states at or near the Fermi level, the photoexcited hole in the metal substrate is completely screened and has little effect on the electron. As a result, one can explain much of the physics of image potential states using models as simple as a one-dimensional atomic-H-like single-electron Hamiltonian to account for the energetics[1] or as sophisticated as multiple-scattering, or many-body theories to explain the dynamics.[2]

What happens when the hole cannot be ignored? It is well known for materials other than metals that the photoexcited hole is not completely screened and the electron-hole interaction leads to the formation of a correlated electron-hole pair called "exciton." In fact, excitons determine many optical and optoelectronic properties of nonmetal solids.[3,4] In optical spectra, excitons appear as sharp transitions below the band gap corresponding to single-particle excitations. Depending on the polarizability of the material, excitons may be strongly bound and localized on one or just a few lattice sites (Frenkel exciton) or weakly bound and delocalized over many lattice sites (Mott-Wannier exciton). The former situation is common in organic (molecular) semiconductors, the latter in inorganic semiconductors. Based on these well-established facts and principles for bulk materials, we predict that excitonic states associated with the image bands must exist at surfaces of nonmetals. For an optical excitation from an occupied state of a solid material to an image potential state above the surface, the unscreened hole should lead to the formation of excitonic states energetically below the image band. Since the electron-hole pairs are bound across an interface, we call these charge transfer (CT) excitons.

In this paper, we focus on image band associated CT excitons on organic semiconductor surfaces. They are, in principle, similar to interfacial CT excitons proposed for organic-organic semiconductor interfaces that are of particular interest to organic photovoltaics (OPV).[5] A key step in the operation of an OPV device is the separation of charge at the organic semiconductor donor/acceptor (D/A) interface, resulting in an electron in the conduction band of the donor and a hole in the valence band of the acceptor. Due to the low dielectric constants of organic materials, charge separation at the D/A interface does not give free charge carriers but rather a bound electron-hole pair across the interface, i.e., a CT exciton. In the present study, we view the image band as similar to the conduction band of the electron acceptor. Thus, the CT excitons on organic semiconductor surfaces can serve as model systems for the understanding of interfacial CT excitons at D/A interfaces.

We probe charge transfer excitons and image potential states on the surfaces of two prototypical crystalline organic semiconductors, pentacene and tetracene, using femtosecond time-resolved (TR) and angle-resolved two-photon photoemission spectroscopy (2PPE).[6] In such a 2PPE experiment, the first photon excites an electron from the valence band (e.g., the highest-occupied molecular orbital or HOMO) into the image potential state or the CT exciton state. After a controlled time delay, the second photon probes the transiently populated state by breaking up the exciton and eject-

 

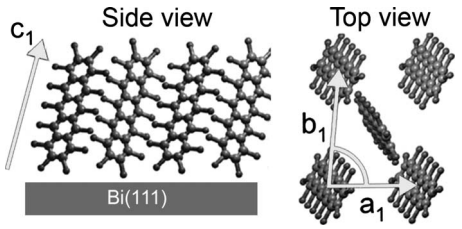


FIG. 1. Schematic illustration of an epitaxial monolayer of pentacene on Bi(111). The three principal axes ($\boldsymbol{a_1}$,$\boldsymbol{b_1}$,$\boldsymbol{c_1}$) of the unit cell are shown as arrows.

ing the photoelectron. A preliminary report of CT excitons on pentacene,[7] a discussion on how CT excitons may participate in the photovoltaic process,[5] and a description of the spectroscopic aspects of probing excitons in 2PPE (Ref. 8) have appeared elsewhere. The present work provides a comprehensive account of CT excitons and image potential states on both pentacene and tetracene surfaces.

## II. EXPERIMENT

### A. Sample preparation

We carried out all experiments in an ultrahigh vacuum chamber with a base pressure lower than $5\times10^{-10}$ mbar. The sample is cooled by liquid nitrogen and heated resistively. We used two types of samples: epitaxial pentacene or tetracene thin films grown on the Bi(111) surface[9] and polycrystalline thin films grown on Si(111).[10,11] In both cases, the substrate (10 mm$\times$5 mm$\times$0.5 mm) was cut from a *p*-type polished Si(111) wafer with a resistivity of 0.5 $\Omega$ cm. The Si sample was degassed at 900 K for 12 h, flashed to $\sim$1510 K for 30 s to remove the native surface oxide, annealed at 1170 K for 120 s, and then slowly cooled down to room temperature. This procedure routinely yielded a well-reconstructed Si(111)-7$\times$7 surface. The Bi(111) surface was formed by vapor deposition of $>$10 monolayers (ML) of Bi from a Knudsen cell onto the Si(111)-7$\times$7 surface at a substrate temperature of 298 K, followed by annealing at 400 K for 1 h.[9] Crystallinity of both Si(111)-7$\times$7 and Bi(111) surfaces was confirmed by low-energy electron diffraction (LEED). The pentacene and tetracene thin films were grown on either the Bi(111) or Si(111)-7$\times$7 surface by vapor deposition from a second Knudsen cell. The sublimation temperatures were 473 and 385 K, and the substrate temperatures 298 and 250 K for pentacene and tetracene, respectively.

Vapor-deposited pentacene is known to grow epitaxially on Bi(111) in the "stand-up" bulklike crystalline form, with the *c* axis (long molecular axis) nearly perpendicular to, and the *ab* plane parallel to the substrate surface, Fig. 1.[9] The LEED pattern for ML pentacene/Bi(111), Fig. 2(a), is actually a superposition of diffraction spots from multiple crystalline domains,[7] due to the large size ($\sim$1 mm) of the electron beam used here. The LEED pattern agrees perfectly with the prediction, Fig. 2(b), constructed from the reciprocal lattice based on known in-plane unit-cell parameters of pentacene ($\boldsymbol{a_1}$=6.06 Å, $\boldsymbol{b_1}$=7.90 Å, and $\boldsymbol{\theta_1}$=85.8°)[12] and taking into account the pseudosixfold rotational symmetry of the Bi(111) surface and chiral twins of pentacene crystalline domains. This result is also in agreement with previous microbeam LEED measurements from a single-crystalline pentacene domain on the Bi(111) surface.[13]

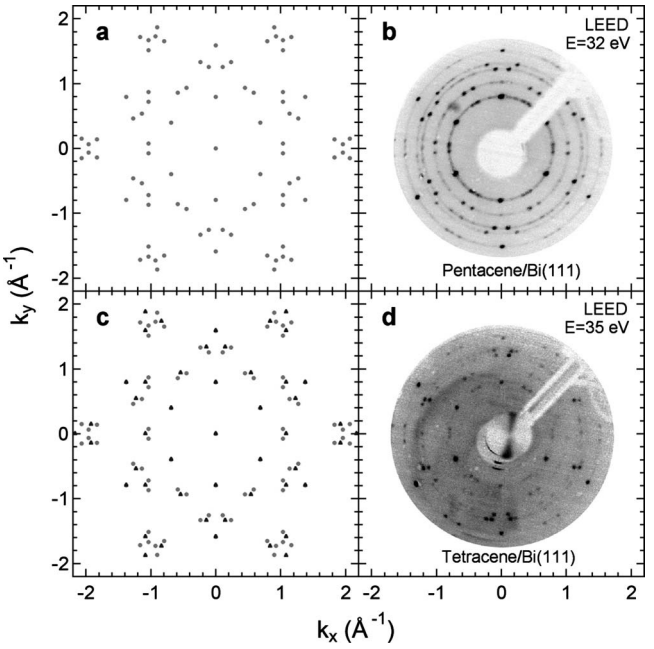


FIG. 2. Experimental low-energy electron-diffraction (LEED) pattern for monolayer (b) pentacene/Bi(111) and (d) tetracene/Bi(111). Panel (a): predicted LEED pattern corresponding to lattice parameters of $\boldsymbol{a_1}$=6.06 Å, $\boldsymbol{b_1}$=7.90 Å, and $\boldsymbol{\theta_1}$=85.8° for pentacene. Panel (c): predicted LEED pattern for monolayer tetracene from the superposition of two crystalline structures, those with $\boldsymbol{a_1}$=6.06 Å, $\boldsymbol{b_1}$=7.90 Å, and $\boldsymbol{\theta_1}$=85.8° (gray circles) and those with $\boldsymbol{a_2}$=5.8$\pm$0.2 Å, $\boldsymbol{b_2}$=7.90 Å, and $\boldsymbol{\theta_2}$=90° (black triangles).

The LEED pattern for monolayer tetracene/Bi(111) is similar to that of pentacene, suggesting that tetracene also grows epitaxially on Bi(111) in the stand-up bulklike crystalline form. Detailed analysis shows that there are two different crystalline forms: the first form is identical to that of pentacene, as shown by the diffraction spots in gray circles in panel (c) with in-plane unit-cell parameters of $\boldsymbol{a_1}$=6.06 Å, $\boldsymbol{b_1}$=7.90 Å, and $\boldsymbol{\theta}$=85.8°. The second form has slightly different in-plane lattice constants, with $\boldsymbol{a_2}$=5.8$\pm$0.2 Å, $\boldsymbol{b_2}$=7.90 Å, and $\boldsymbol{\theta_2}$=90°, as shown by triangle diffraction spots in (c). While both structures share the same $\boldsymbol{b}$ vector due to a point-on-line matching with the underlying Bi(111) lattice, the $\boldsymbol{a_2}$ vector is different. In the second form, $\boldsymbol{a_2}$ forms a right angle with $\boldsymbol{b_2}$ and is slightly shorter than that of the first form. Since intermolecular interaction in the herringbone packed layer of tetracene is expected to be weaker than that of pentacene, the molecule-substrate surface interaction and, thus, lattice matching to the Bi(111) substrate are relatively more important.

For multilayer pentacene or tetracene thin films grown on the clean silicon surface, it is known that strong molecule-surface interaction results in a chemisorbed first layer with lying-down geometry. Subsequent deposition beyond this wetting-layer results in the stand-up bulklike polycrystalline structure.[11] The polycrystalline morphology of the multilayer film appears as ring patterns in LEED (data not shown) but

the in-plane lattice parameters ($\boldsymbol{a}$,$\boldsymbol{b}$) agree with those of the bulk crystal.

We calibrate the pentacene or tetracene growth rate by analyzing two-photon photoemission spectra (see below) and assign ML coverage as the threshold when spectral features from the clean Bi(111) surface disappear. Multilayer coverage on either Bi(111) or Si(111) is then estimated from this calibrated growth rate. This procedure likely underestimates the pentacene or tetracene coverage as islands of the second layer start to form on top of the first layer before the latter is complete.

### B. Two-photon photoemission spectroscopy

The 2PPE experimental setup has been detailed elsewhere.[14] The third harmonic (~0.1 nJ/pulse) and the fundamental (~1 nJ/pulse) output of a femtosecond Ti:sapphire oscillator (Coherent, 700–900 nm tuning range, <100 fs pulse width, 76 MHz repetition rate) were used as pump and probe pulses, respectively. Photoelectrons were detected in a VG-100AX hemispherical electron energy analyzer with energy resolution of approximately 35 meV. To align the vacuum levels of the sample and the analyzer, a negative bias voltage was applied to each sample.

2PPE spectra are naturally referenced to the Fermi level $E_F$ of the instrument. For metallic samples, the Fermi levels of sample and instrument align, and occupied states near the Fermi level provide a clear energy reference in the measured spectrum. However, in the case of the Si substrate the energy reference is more difficult to determine due to possible band bending at the surface and contact voltage at the sample holder. As described in Sec. III, we overcome this limitation by referencing the spectra to the vacuum level $E_{vac}$ which is more easily accessible in the measured spectrum. The binding energy $E_B$ referenced to the vacuum level is then related to the Fermi-level referenced energy scale via the work function $\varphi = E_{vac} - E_F$, according to

$$E - E_F = \phi - E_B. \quad (1)$$

Since the UV photon energy used was greater than the surface work function, there was one-photon photoemission from the sample. We found that the 2PPE spectrum remained constant for pump-probe delay time longer than 1 ps; it consisted exclusively of one-photon photoemission, as verified by blocking the IR probe-laser light. To accurately analyze each 2PPE spectrum, we subtracted the one-photon photoemission contribution using the 2PPE spectrum taken at a pump-probe delay of 3 ps. Except for angle-resolved measurements, all spectra were taken at normal emission. In angle-resolved 2PPE experiments, we rotated the sample to vary the angle of electron detection. Most 2PPE spectra presented here were recorded at a sample temperature of ~120 K. In the case of pentacene thin films, we have varied the sample temperature in the range of 120–300 K and found no significant difference in the energetics and dynamics of IPS and CTE states.

Before presenting the results, we first illustrate what we expect to see in a 2PPE spectrum. We use 2PPE spectroscopy to probe the IPS and CTE on two types of surfaces: epitaxial monolayer and multilayers of pentacene or tetracene on the Bi surface, and multilayers of the same molecules on Si. For monolayer pentacene or tetracene on Bi while a CTE can only be excited from the HOMO band of the molecule (creating a hole in the HOMO and an electron in the CTE state), an IPS can be excited from either the HOMO or an occupied state of the Bi substrate depending on photon energy. For thicker films, the spatial overlap of the IPS wave function with those of the substrate (Bi or Si) becomes negligible and both CTE and IPS can only be excited from the HOMO. These situations are illustrated in Fig. 3. Note that the two different mechanisms for the populations of the image potential states are reflected in the dynamics. In the direct mechanism (right), the IPS is populated instantaneously by the pump-laser pulse ($h\nu_1$) while in the indirect mechanism there is a time delay between the population of the IPS and $h\nu_1$. This time delay is indeed observed for the IPS on monolayer pentacene covered Bi(111).

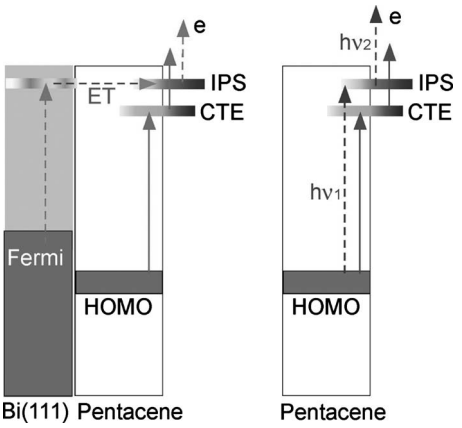


FIG. 3. Schematic illustration of the 2PPE processes on monolayer pentacene/Bi (left) or multilayer pentacene (right) surfaces. The dashed arrows represent the indirect mechanism for populating the IPS via electron transfer from the substrate. This mechanism is suppressed in multilayer pentacene films. In the multilayer sample, higher photon energy is required to populate the IPS from the pentacene HOMO.

## III. RESULTS AND DISCUSSIONS

### A. Numerical simulation

To aid the assignment of IPS and CT exciton states on pentacene and tetracene surfaces, we first review numerical simulation in a simplistic dielectric continuum model: a localized hole at an organic semiconductor surface and a free electron on the vacuum side. The assumption of a fixed, localized hole is justified because the HOMO band of pentacene or tetracene is nearly flat near the Γ point, corresponding to heavy effective hole mass.[15,16] The dielectric continuum approximation is chosen for practical reasons since microscopic treatments are intractable at present. As will be shown below, it reasonably explains the observed IPS and CTE states. Within this model, the single-particle Hamiltonian of the electron is

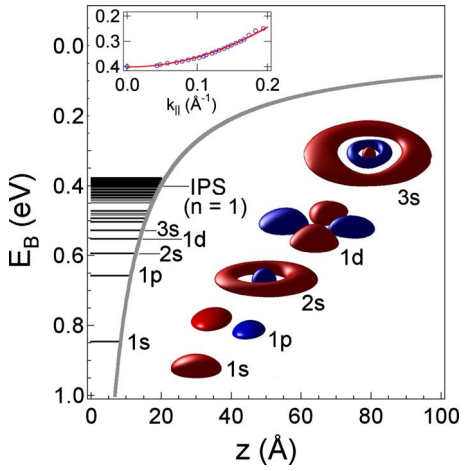


FIG. 4. (Color online) Numerical solution to Eq. (2) with $z_h = -2.7$ Å. The delocalized $n=1$ IPS band is located at binding energy $E_B \leq 0.4$ eV and the localized CTEs are at $E_B > 0.4$ eV. The inset shows the parallel dispersion of the $n=1$ IPS. Also shown are wave functions (in the $xy$ plane) for the five lowest-energy CTE states.

$$\hat{H} = -\frac{\hbar^2}{2m_e}\nabla^2 - \frac{\beta e^2}{4\pi\varepsilon_o z} - \frac{\gamma e^2}{4\pi\varepsilon_o\sqrt{x^2+y^2+(z-z_h)^2}}, \quad (2)$$

where $z$ is the surface normal with the image plane at $z=0$ and the hole at $(0,0,z_h)$. $\beta=(\varepsilon-1)/(\varepsilon+1)$ and $\gamma=2/(\varepsilon+1)$ account for screening of the charges[17] and $\varepsilon=5.3$ is the dielectric constant of pentacene.[18] $\varepsilon_o$ is the vacuum permittivity and $e$ is the electron charge. We solve the Schrödinger equation numerically using the finite element method within the COMSOL simulation software. These calculations return the energy eigenfunctions and eigenvalues that can be divided into two regions, Fig. 4. The first region with binding energy $E_B \leq 0.4$ eV is a band of delocalized states corresponding to the $n=1$ IPS (see the parallel dispersion curve in the inset of Fig. 4). The second region ($E_B > 0.4$ eV) consists of a series of localized CTE states, with some of the wave functions shown in the figure. Perhaps the most important distinction of the CTE from the IPS is that the latter is delocalized (in the surface plane) and corresponds to a two-dimensional free-electron continuum. The atomic hydrogen-like CT exciton states bear resemblance to $\sigma$ and $\pi$ resonances for adsorbed alkali atoms on noble-metal surfaces, as shown recently by Petek and co-workers.[19,20] An excess electron in such an adsorbate resonance is bound by the composite image potentials, as well as the positively charged ionic core of the adsorbed alkali atom. Note that in the adsorbed alkaline atom system, the positive charge (ionic core) is outside of the surface and one needs to include the image potential of the positive charge in constructing the Hamiltonian.[19,20] It is different from Eq. (2) for the CT exciton where the positive charge is inside the surface and the effect of the interface is simply reflected in the $\beta$ factor.[17]

### B. Epitaxial pentacene/Bi(111)

Figure 5 shows two sets of 2PPE spectra of pentacene/Bi(111) at the indicated pump photon energies. The spectra

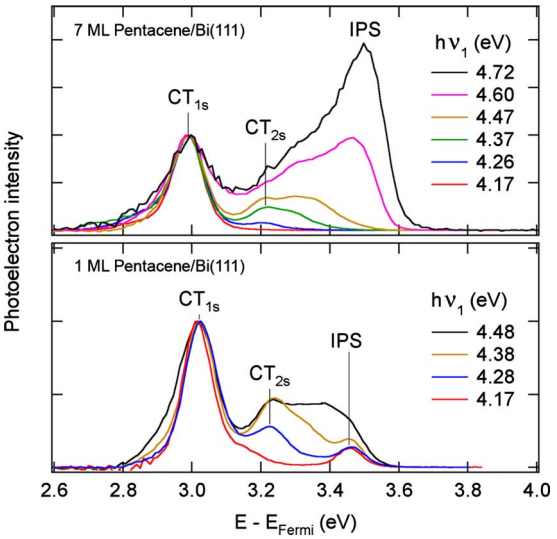


FIG. 5. (Color online) 2PPE spectra from (a) monolayer pentacene/Bi and (b) multilayer pentacene/Bi surfaces, with increasing pump photon energy from bottom to top. The 2PPE intensities are normalized by the peak value of CT-1$s$, and the energy positions of CT-1$s$ and IPS are indicated.

in the lower panel are taken on 1 ML pentacene/Bi(111). At the lowest pump photon energy, $h\nu_1=4.17$ eV, we observe two distinct peaks resulting from the transient population of two unoccupied states at energies of 3.02 and 3.46 eV, respectively, above the Fermi level. As detailed in our preliminary paper,[7] these two peaks correspond to the 1$s$ CT exciton and the $n=1$ IPS. The electron densities $|\psi|^2$ of both states are concentrated in the vacuum above the surface; physisorption of a layer of molecular dielectric, $n$-nonane ($C_9H_{20}$), onto the 1 ML pentacene/Bi quenches both peaks. The initial state of the CTE peak is the HOMO of pentacene which lies $\sim$1.2 eV below the Fermi level.[16] Thus, the 4.17 eV photon energy is in resonance with the HOMO$\rightarrow$CT$_{1s}$ transition. In contrast, the initial state of the IPS at this photon energy lies in the HOMO-LUMO gap of pentacene and must be located in the Bi substrate. Indeed, the IPS peak disappears at this photon energy for film thickness above 1 ML, as the probability of electron transfer from the Bi substrate vanishes. When $h\nu_1$ increases to 4.28, 4.38, and 4.48 eV, we see more CT excitons come into resonance. Among these hot CT excitons, only the CT$_{2s}$ is distinctively observed. All other CT excitons are not resolved due to spectral congestion. The hot CT excitons can decay into lower-lying ones, as will be presented below. The work function determined from the vacuum edge is 3.96 eV, consistent with ultraviolet photoemission results.[16] Given this value, the binding energies of the states with respect to the vacuum level are CT$_{1s}$=0.92, CT$_{2s}$=0.74, CT$_{3s}$=0.58, and IPS=0.50 eV. The quantitative results are summarized in Table I.

As the CT excitons are formed at the surface of the pentacene thin film via photoexcitation from the HOMO, their formation is insensitive to film thickness. The upper panel in Fig. 5 shows a set of 2PPE spectra from 7 ML pentacene/Bi at the indicated photon energy energies ($h\nu_1=4.17$–4.77 eV). Again, at the lowest $h\nu_1$ (=4.17 eV) only the CT$_{1s}$

TABLE I. Binding energies and lifetimes of the CT excitons and IPS.

| Surface and work function | State | Binding energy (eV) | Lifetime (fs) |
|---|---|---|---|
| Monolayer Pc/Bi $\phi$=3.96 eV | CT1$s$ | 0.94±0.02 | 60±10 |
| | CT2$s$ | 0.74±0.02 | 35±10 |
| | CT3$s$ | 0.58±0.02 | 55±10 |
| | IPS ($n$=1) | 0.50±0.02 | 135±10 |
| Multilayer Pc/Bi $\phi$=3.91 eV | CT1$s$ | 0.92±0.02 | 100±20 |
| | CT2$s$ | 0.59±0.02 | 70±10 |
| | CT3$s$ | 0.46±0.05 | 55±10 |
| | IPS ($n$=1) | 0.39±0.02 | 95±10 |
| Multilayer Pc/Si $\phi$=4.40 eV | CT1$s$ | 0.87±0.02 | 100±10 |
| | CT2$s$ | 0.65±0.02 | 70±10 |
| | CT3$s$ | 0.44±0.02 | 110±10 |
| | IPS ($n$=1) | 0.35±0.02 | 220±20 |
| | IPS ($n$=2) | 0.09±0.02 | 250±20 |
| Monolayer Tc/Bi $\phi$=3.98 eV | IPS ($n$=1) | 0.42±0.02 | 460±20 |
| Multilayer Tc/Si $\phi$=4.40 eV | CT1$s$ | 0.91±0.02 | 120±10 |
| | CT2$s$ | 0.63±0.02 | 50±10 |
| | CT1$d$ | 0.54±0.02 | 840±80 |
| | IPS ($n$=1) | 0.32±0.02 | 760±80 |

exciton is populated. With increasing photon energy, the $CT_{2s}$ and then higher-lying CT excitons come into resonance. At the highest pump photon energy ($h\nu_1$=4.77), the $n$=1 image potential state also comes into resonance. In this case, similar to the CT excitons, the IPS is also populated by photoexcitation from the HOMO. However, in contrast to the CT excitons, the excited electrons have sufficient energy to escape the potential well due to the hole in the HOMO. Note that, unlike the observation on 1 ML pentacene/Bi, transfer of photoexcited electrons from the Bi substrate into the IPS is negligible for pentacene film thickness ≥2 ML, and thus, the IPS peak is not observed at photon energies below the HOMO→IPS resonance.

Figure 6 shows a complete view of the CT excitons and the $n$=1 IPS on 1 ML pentacene/Bi in time, energy, and momentum spaces. The right panel is a pseudocolor representation of parallel dispersion from angle-resolved measurements. The IPS clearly exhibits a parabolic dispersion curve which corresponds to an effective electron mass of $m_{\text{eff}} \sim 1.5m_e$ whereas the $CT_{1s}$, $CT_{2s}$, and $CT_{3s}$ states show no measurable dispersion, which clearly sets them apart from the dispersive IPS. Lack of dispersion of the CTE peaks can have several reasons. First, it may be an effect of the spatial localization of the CTE. Second, however, it has to be noted that in probing the electron the photoemission process breaks up the exciton. The momentum vector of the exciton is not preserved in the emitted electron, as the hole can carry away with an undetermined amount of momentum. Even if a CT exciton possesses delocalization in the surface plane (due to the delocalization of the hole in the HOMO band), the photoemitted electron may show no dispersion.

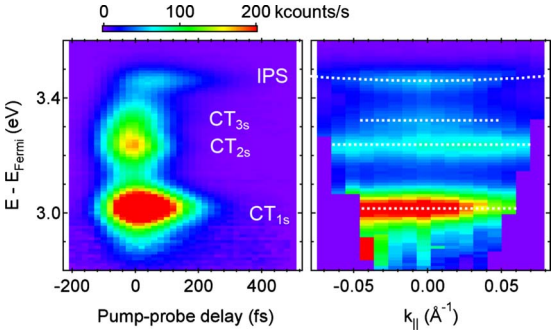


FIG. 6. (Color online) Pseudocolor plot of time-resolved (left) and angle-resolved (right) 2PPE spectra for monolayer pentacene/Bi(111) taken at a pump photon energy of $h\nu_1$=4.38 eV. The spectra in the right panel were recorded at a pump-probe delay time of 80 fs for improved energy resolution.

The left panel in Fig. 6 is a pseudocolor plot of 2PPE spectra taken at different pump-probe time delays. Each vertical cut is a 2PPE spectrum taken at a particular pump-probe delay while each horizontal cut is a pump-probe cross-correlation (CC) curve at a particular electron energy. All the CT excitons are short lived (lifetimes <100 fs) because they are referenced to the high-lying image state and can readily decay into Frenkel excitons within the organic semiconductor.

The dynamics of creation and decay of the IPS and the CT excitons can be obtained from analysis of the CC curves. We analyze each CC curve using a simple rate equation model involving a convolution of an exponential response function and the temporal profile of the pump pulse. This simple model is the limiting case of the more rigorous optical Bloch equations if the dephasing time is much shorter than the laser-pulse width.[21] The correlation function is obtained as the solution of the differential equation

$$\frac{dN}{dt} = R \cdot I_{\text{pump}}(t - t_o) - \frac{N}{\tau}, \tag{3}$$

where $N(t)$ is the intermediate-state population; $I_{\text{pump}}$ is the pump-pulse profile, and $t_o$ is time zero (center of the pump pulse); $R$ is a proportionality constant which contains the excitation cross-section and initial-state density; $\tau$ is the intermediate-state decay time constant. The CC curve of photoelectron intensity is then obtained by the convolution of $N(t)$ with the temporal profile of the probe pulse (well described by a Gaussian pulse shape) and the photoionization cross section (assumed to be constant). Practically, the last convolution step is often not necessary if the associated broadening can be included in (and is indistinguishable from) the pump-pulse width.

Figure 7 shows CC curves for various states probed at two pump photon energies for 1 ML pentacene/Bi(111). At the lower photon energy which is in resonance with the HOMO→$CT_{1s}$ transition, only the $CT_{1s}$ state is excited. Fitting the CC curve to Eq. (3) shows that $CT_{1s}$ is populated directly by $h\nu_1$ at $t_0$=0 and decays with a time constant of $\tau$=56±10 fs. However, fitting the CC curve of the IPS requires an effective delay of $t_0$=44±10 fs. We believe this is

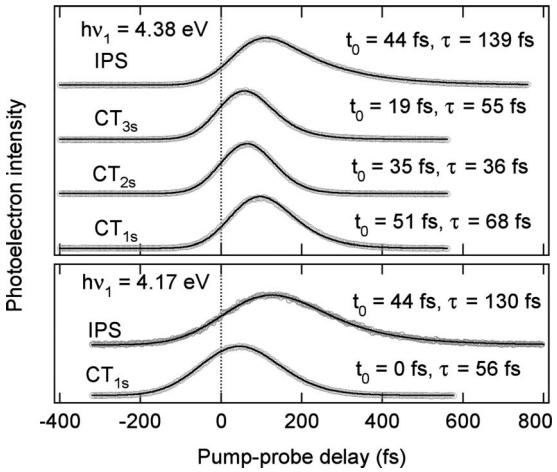


FIG. 7. 2PPE cross-correlation curves of the CT excitons and the IPS on 1ML pentacene/Bi(111) measured at $h\nu_1$=4.17 eV (lower) and 4.38 eV (upper). We determine the transient state lifetimes by fitting to the rate equation model using a Gaussian pulse profile. $t_0$ is the temporal offset of the Gaussian with respect to zero pump-probe delay and $\tau$ is the exponential decay time. Dots represent raw data and solid lines are fits. The curves are normalized and vertically offset for clarity.

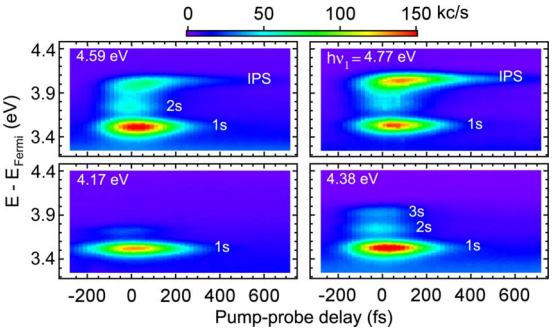


FIG. 8. (Color online) Pseudocolor plot of time-resolved 2PPE spectra taken at the indicated photon energies ($h\nu_1$=4.17–4.77 eV) for multilayer pentacene (>10 nm) deposited on Si(111). The electron energy scale is referenced to the Fermi level.

a result of the indirect mechanism: photoexcitation in the Bi substrate or at the Bi/pentacene interface, followed by electron transfer through the 1.5-nm-thick pentacene film to the IPS on the pentacene surface. A more rigorous analysis requires the addition of a source term in Eq. (3) but is not feasible quantitatively in the absence of detailed knowledge of the initial photoexcitation step.

At $h\nu_1$=4.38 eV, CT excitons above $CT_{3s}$ are resonantly excited. The highly excited states relax down the CT exciton manifold, as evidenced by the sequential increase in the delay time ($t_0$=19, 35, and 51 fs for 3*s*, 2*s*, and 1*s*, respectively). This increase in the apparent delay times for populating lower-lying states is a qualitative measure of the relaxation rate from a higher-lying CT exciton state to a lower-lying one. This is in agreement with a common rule in molecular photophysics: highly excited singlet electronic states often quickly relax to lower-lying ones.

### C. Polycrystalline pentacene on Si(111)

The IPS and CT exciton states are also observed on polycrystalline pentacene thin films formed on Si(111). An advantage of the silicon substrate over Bi is the much reduced interference from one-photon photoemission. On the other hand, the correct energy scale is more difficult to establish due to the lack of spectral features from the substrate. For this reason, we reference the energy scale to the vacuum level which is determined from measured image state energies as described below. The pseudocolor plots in Fig. 8 show TR-2PPE spectra taken at different pump-probe time delays from multilayer pentacene (>10 nm) on Si(111) at the indicated photon energies ($h\nu_1$=4.17–4.77 eV). The presentation of two-dimensional data in both time and energy domains allows us to more clearly identify the CT exciton states. At the lowest photon energy, $h\nu_1$=4.17 eV, the spectrum is dominated by the $CT_{1s}$ peak. With increasing photon energy, we see hot CT excitons, particularly the well-resolved $CT_{2s}$ and $CT_{3s}$, come into resonance. As $h\nu_1$ is increased to 4.59 eV and above, we also observe the image states. At the highest photon energy ($h\nu_1$=4.77 eV), in particular, we observe both $n$=1,2 image potential states. This is more obvious in the individual spectra shown in Fig. 9. There is photoelectron intensity at energy above 4.2 eV at $h\nu_1$=4.77 eV. The upper panel reproduces this, with the low binding-energy region scaled by a factor 20 to clearly reveal a distinct peak assigned to the $n$=2 IPS. Also shown in the graph are peaks of $CT_{1s}$, $CT_{2s}$, $CT_{3s}$, and the $n$=1 IPS obtained from decomposition.

The observation of two IPS provides an alternative energy reference since these states naturally align to the vacuum level. On a dielectric surface, the binding energies of the image potential states are given by

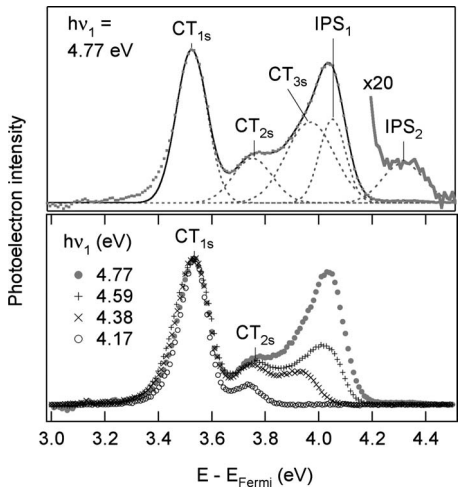


FIG. 9. Lower: 2PPE spectra for 7 ML pentacene/Si(111) taken at zero pump-probe delay and the indicated photon energies ($h\nu_1$=4.17–4.77 eV). The spectrum at $h\nu_1$=4.77 eV is reproduced in the upper panel, with the spectral region at binding energy ≤0.2 eV scaled by 20×. Also shown is the decomposition (dashed curves).

$$E_{B,n} = \frac{0.85\ \text{eV}}{(a+n)^2} \cdot \left(\frac{\varepsilon - 1}{\varepsilon + 1}\right)^2, \tag{4}$$

where $n=1,2$ is the quantum number; $\varepsilon$ (=5.3 for pentacene) is the dielectric constant; $a$ is the so-called quantum defect and is related to penetration of the image state wave function into the dielectric material (i.e., deviation from a hard wall at the pentacene/vacuum interface). Fitting the experimentally determined energetic positions of the $n=1,2$ states to Eq. (4) yields the vacuum level with respect to the instrument Fermi level (4.40 eV) and a small quantum defect of $a=0.06$. The binding energies of the CT excitons and IPS states are $CT_{1s}=0.87$ eV, $CT_{2s}=0.65$ eV, $CT_{3s}=0.44$ eV, $IPS_1=0.35$ eV, and $IPS_2=0.09$ eV. The first four values are in close agreement with numerical simulations in Fig. 4. Note that Eq. (4) does not correctly describe the monolayer system discussed in the previous section. There, we found that the $IPS_1$ binding energy is 0.15 eV larger. This additional binding energy occurs due to the proximity of the highly polarizable bismuth substrate. By the same account, the CTE energies are affected not as much since the CTE consists of an electron and a hole which induce polarization of opposite sign. Located further away from the Bi/pentacene interface, the hole is better screened than the electron, which results in a slightly weaker binding energy on the monolayer than on the multilayer system.

Similar to the monolayer surface, the IPS and CT exciton states on the polycrystalline pentacene surface are short lived. Cross-correlation analysis of data in Fig. 8 yields transient state lifetimes of $220\pm20$ fs and $250\pm20$ fs for the $n=1$ and 2 IPS, respectively. The lifetimes of the CT excitons are $\tau=100\pm10$ fs, $70\pm10$ fs, and $110\pm10$ fs, for the $CT_{1s}$, $CT_{2s}$, and $CT_{3s}$, respectively. Since the image potential states are less bound than the CT excitons, we expect $|\psi|^2$ of an IPS to be further into the vacuum and possess a longer lifetime than those of a CT exciton. A more quantitative understanding of the differences in these lifetimes requires theoretical analysis of dynamics in the IPS and CTEs; this is a formidable task at the present time.

### D. Tetracene

Image potential states or resonances can exist on all polarizable surfaces. Similarly, we predict that CT excitons should be general to organic semiconductor surfaces, given the relatively narrow valence-band width and the localization of the hole. In addition to pentacene, we have investigated the IPS and CT excitons on a closely related organic semiconductor, tetracene. We first focus on monolayer epitaxial tetracene/Bi(111).

On the monolayer tetracene/Bi surface, TR-2PPE measurement only reveals the image potential state, not the CT excitons. This is shown in the pseudocolor representation in Fig. 10. The identity of the $n=1$ IPS is verified by the free-electronlike parallel dispersion in the right panel. Note that the short-lived feature at energy above the IPS on tetracene is the $n=1$ image state on small areas of bare Bi(111) surface.[22] The work function of the monolayer tetracene covered surface is $\phi=3.98$ eV. This gives a binding energy of 0.42 for the $n=1$ image potential state. The $n=1$ IPS is relatively long lived, $\tau=460\pm20$ fs; we believe it is energetically located in the gaps of LUMO+$x$ bands of tetracene.

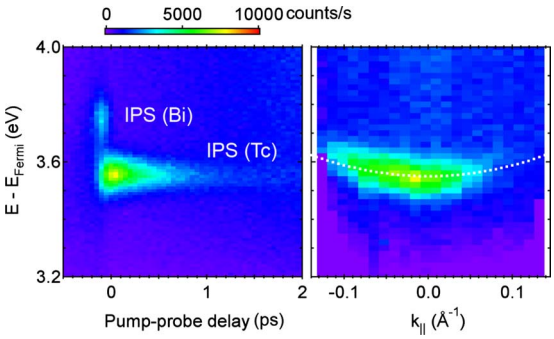


FIG. 10. (Color online) Pseudocolor plot of angle-resolved (right) and time-resolved (left) 2PPE spectra for monolayer tetracene/Bi(111) taken at a pump photon energy of $h\nu_1=4.17$ eV. The spectra in the right panel were recorded at a zero pump-probe delay time. The dashed curve is free-electron dispersion.

As on monolayer pentacene/Bi, the IPS on monolayer tetracene/Bi(111) is populated via indirect photoexcitation from Bi states at or near the Fermi level. The HOMO of tetracene lies deeper in energy than that of pentacene and is estimated to be ~1.3 eV below the Fermi level.[23,24] Based on the estimated positions of CT excitons, we need photon energies more than 0.1 eV higher than that used in Fig. 10 to reach the CT exciton resonances but a higher photon energy results in a dramatic increase in the interfering one-photon photoemission signal. Analogously to the pentacene experiments, we turn to tetracene thin films deposited on the Si(111) substrate to overcome difficulties due to intense one-photon photoemission and reference the binding-energy scale according to the observed energy position of the IPS and Eq. (4), using a dielectric constant of $\varepsilon=4.7$ for tetracene[18,25] and assuming the same small quantum-defect parameter ($a=0.06$) as determined for pentacene.

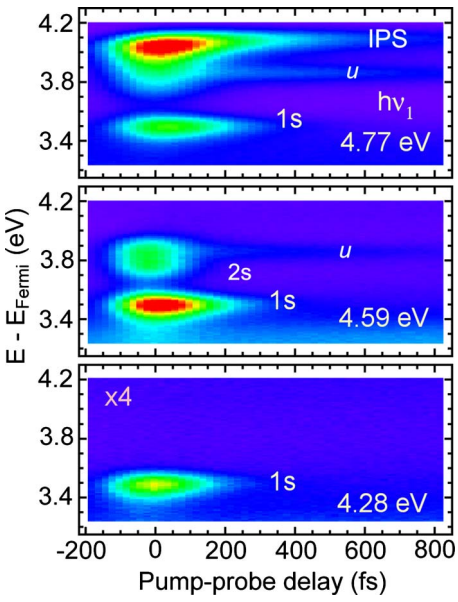


FIG. 11. (Color online) Pseudocolor plot of time-resolved 2PPE spectra taken at the indicated photon energies ($h\nu_1=4.17$–4.77 eV) for multilayer tetracene (>10 nm) deposited on Si(111).

Figure 11 shows pseudocolor plots of TR-2PPE spectra taken at different pump-probe time delays from multilayer tetracene (>10 nm) on Si(111) at the indicated photon energies ($h\nu_1$=4.17–4.77 eV). Similar to the observation on polycrystalline pentacene, we again see a series of CT excitons coming into resonance with increasing pump photon energy. The binding energies and decay times (in parentheses) of these states are $CT_{1s}$ (0.91 eV, 120±10 fs); $CT_{2s}$ (0.63 eV, 50±10 fs); "*u*" (0.54 eV, 840±80 fs); and the $n$=1 IPS (0.32 eV, 760±80 fs). The peak labeled *u* at 0.09 eV above $CT_{2s}$ stands out for its long lifetime. This is at a similar energetic position as the $CT_{1d}$ state predicted from the dielectric continuum model in Fig. 4. The unusually long lifetime may be related to its symmetry which inhibits the decay into a Frenkel exciton in tetracene or lower-lying CT exciton state at the surface. In principle, photoemission in the surface-normal direction should be forbidden for states with in-plane nodes. However, the multilayer tetracene thin deposited on Si(111) is polycrystalline in nature. The polycrystallinity and disorder should relax the selection for photoemission.

### E. Quantitative summary

The experimentally determined binding energies and lifetimes of the CT excitons and image potential states are summarized in Table I. Note that the surface work function on multilayer Pc/Si is higher than that on the multilayer Pc/Bi; the difference may be attributed to band bending at the Pc/Si interface.

## IV. CONCLUSIONS

This account establishes another type of optical excitation, i.e., charge transfer excitons, on organic semiconductor surfaces. While image potential states or resonances can exist on all polarizable surfaces because of the universal nature of the image potential, CT excitons are of general significance to nonmetal surfaces if the photogenerated hole is localized to the surface region and is not completely screened by the dielectric response of the material. This is a common situation in organic semiconductors with relatively narrow valence-band width. In the examples presented here, crystalline pentacene and tetracene surfaces, we show the presence of both image potential states and charge transfer excitons. The IPS is essentially an upper limit of CTEs where the electron is no longer confined by the electron-hole Coulomb potential and is bound by the image potential only. The binding energies of these states agree well with solutions to the atomic-H-like Schrödinger equation based on the image potential and the electron-hole Coulomb potential.

## ACKNOWLEDGMENTS

This work was supported by the National Science Foundation under Grant No. DMR-0804583. Support by the Minnesota Supercomputer Institute and the MRSEC Program of the National Science Foundation under Grant No. DMR-0212302 is also acknowledged.

*Author to whom correspondence should be addressed. Present address: Department of Chemistry & Biochemistry, University of Texas, Austin, TX 78712. zhu@cm.utexas.edu

[1] P. M. Echenique and J. B. Pendry, Prog. Surf. Sci. **32**, 111 (1989).
[2] P. M. Echenique, R. Berndt, E. V. Chulkov, Th. Fauster, A. Goldmann, and U. Höfer, Surf. Sci. Rep. **52**, 219 (2004).
[3] Y. Toyozawa, *Optical Processes in Solids* (Cambridge University Press, Cambridge, 2003).
[4] K. S. Song and R. T. Williams, *Self-Trapped Excitons* (Springer, Berlin, 1996).
[5] X. -Y. Zhu, Q. Yang, and M. Muntwiler, Acc. Chem. Res. (to be published).
[6] C. D. Lindstrom and X.-Y. Zhu, Chem. Rev. (Washington, D.C.) **106**, 4281 (2006).
[7] M. Muntwiler, Q. Yang, W. A. Tisdale, and X.-Y. Zhu, Phys. Rev. Lett. **101**, 196403 (2008).
[8] M. Muntwiler, Q. Yang, and X.-Y. Zhu, J. Electron Spectrosc. Relat. Phenom. (to be published).
[9] J. T. Sadowski, T. Nagao, S. Yaginuma, Y. Fujikawa, A. Al-Mahboob, K. Nakajima, T. Sakurai, G. E. Thayer, and R. M. Tromp, Appl. Phys. Lett. **86**, 073109 (2005).
[10] K. S. Yong, Y. P. Zhang, S. W. Yang, P. Wu, and G. Q. Xu, J. Phys. Chem. C **111**, 4285 (2007).
[11] F.-J. Meyer zu Heringdorf, M. C. Reuter, and R. M. Tromp, Nature (London) **412**, 517 (2001).
[12] R. B. Campbell, J. M. Robertson, and J. Trotter, Acta Crystallogr. **14**, 705 (1961).
[13] A. Al-Mahboob, J. T. Sadowski, T. Nishihara, Y. Fujikawa, Q. K. Xue, K. Nakajima, and T. Sakurai, Surf. Sci. **601**, 1304 (2007).
[14] C. D. Lindstrom, D. Quinn, and X.-Y. Zhu, J. Chem. Phys. **122**, 124714 (2005).
[15] K. Hummer and C. Ambrosch-Draxl, Phys. Rev. B **72**, 205205 (2005).
[16] H. Kakuta, T. Hirahara, I. Matsuda, T. Nagao, S. Hasegawa, N. Ueno, and K. Sakamoto, Phys. Rev. Lett. **98**, 247601 (2007).
[17] J. D. Jackson, *Classical Electrodynamics* (John Wiley & Sons, New York, 1975).
[18] E. V. Tsiper and Z. G. Soos, Phys. Rev. B **68**, 085301 (2003).
[19] J. Zhao, N. Pontius, A. Winkelmann, V. Sametoglu, A. Kubo, A. G. Borisov, D. Sanchez-Portal, V. M. Silkin, E. V. Chulkov, P. M. Echenique, and H. Petek, Phys. Rev. B **78**, 085419 (2008).
[20] A. G. Borisov, V. Sametoglu, A. Winkelmann, A. Kubo, N. Pontius, J. Zhao, V. M. Silkin, J. P. Gauyacq, E. V. Chulkov, P. M. Echenique, and H. Petek, Phys. Rev. Lett. **101**, 266801 (2008).
[21] T. Hertel, E. Knoesel, M. Wolf, and G. Ertl, Phys. Rev. Lett. **76**, 535 (1996).
[22] M. Muntwiler and X.-Y. Zhu, New J. Phys. **10**, 113018 (2008).
[23] B. Jaeckel, T. Lim, A. Klein, and W. Jaegermann, Langmuir **23**, 4856 (2007).
[24] C. D. Lindstrom, M. Muntwiler, and X.-Y. Zhu, J. Phys. Chem. B **111**, 6913 (2007).
[25] Z. G. Soos, E. V. Tsiper, and R. A. Pascal, Chem. Phys. Lett. **342**, 652 (2001).